

CLQ: CROSS-LAYER GUIDED ORTHOGONAL-BASED QUANTIZATION FOR DIFFUSION TRANSFORMERS

Kai Liu^{1*}, Shaoqiu Zhang^{1*}, Linghe Kong^{1†}, Yulun Zhang^{1†}

¹Shanghai Jiao Tong University

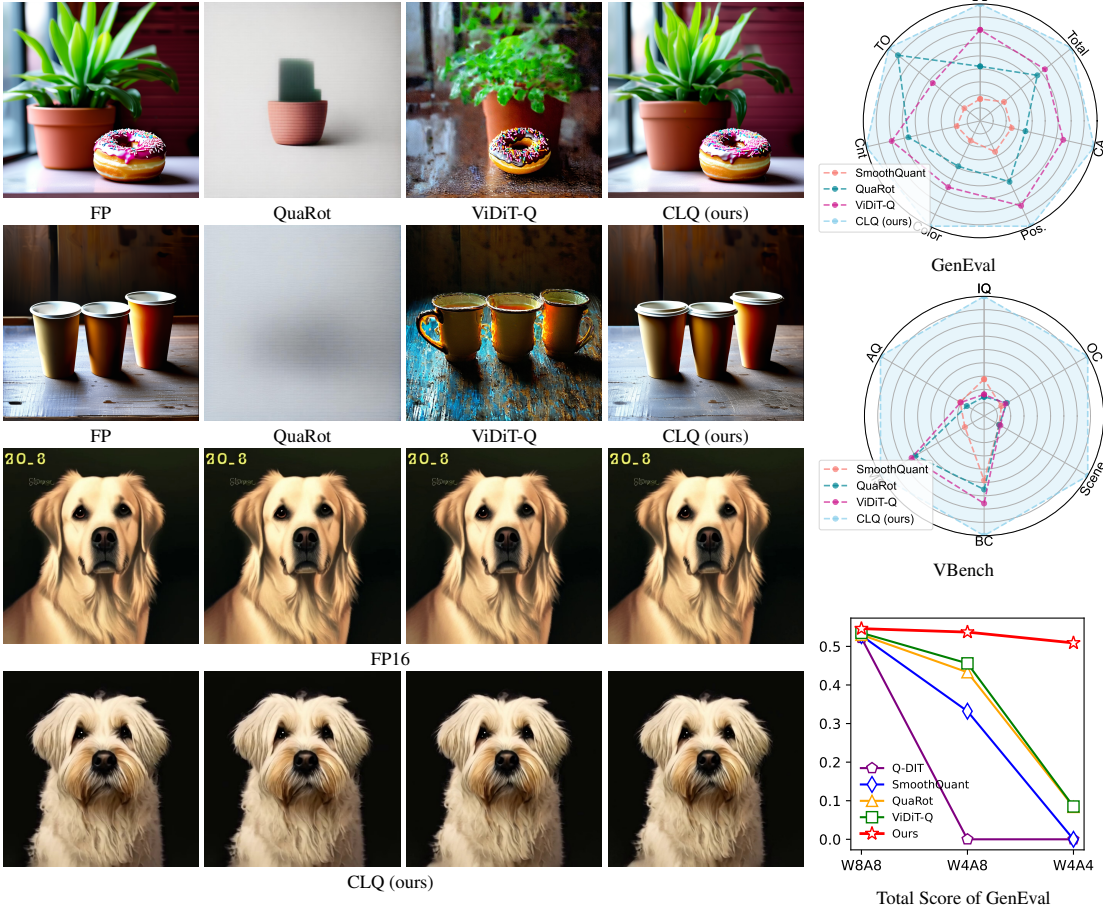


Figure 1: CLQ is a post-training quantization framework for DiTs on visual generation tasks. CLQ could compress the DiTs into W4A4 while preserving the high-quality output of the original model.

ABSTRACT

Visual generation quality has been greatly promoted with the rapid advances in diffusion transformers (DiTs), which is attributed to the scaling of model size and complexity. However, these attributions also hinder the practical deployment of DiTs on edge devices, limiting their development and application. Serve as an efficient model compression technique, model post-training quantization (PTQ) can reduce the memory consumption and speed up the inference, with inevitable performance degradation. To alleviate the degradation, we propose **CLQ**, a cross-layer guided orthogonal-based quantization method for DiTs. To be specific, **CLQ** consists of three key designs. First, we observe that the calibration data used by most of the PTQ methods can not honestly represent the distribution of the activations. Therefore, we propose cross-block calibration (CBC) to obtain accurate calibration data, with which the quantization can be better guided. Second, we propose orthogonal-based smoothing (OBS), which quantifies the outlier score

*Equal contribution

†Corresponding authors: Yulun Zhang, yulun100@gmail.com, Linghe Kong, linghe.kong@sjtu.edu.cn

of each channel and leverages block Hadamard matrix to smooth the outliers with negligible overhead. Third, we propose cross-layer parameter searching (CLPS) to search. We evaluate **CLQ** with both image generation and video generation models and successfully compress the model into W4A4 with negligible degradation in visual quality and metrics. **CLQ** achieves 3.98x memory saving and 3.95x speedup. Our code is available at <https://github.com/Kai-Liu001/CLQ>.

1 INTRODUCTION

Recent advances in visual generation have demonstrated remarkable progress in producing high-quality and photorealistic images and videos (Singer et al., 2022). In particular, diffusion-based models have rapidly become the dominant paradigm in terms of fidelity, diversity, and controllability. More recently, diffusion transformers (DiTs) (Peebles & Xie, 2023) have further pushed the frontier by combining the strong generative capacity of diffusion processes. With the scalability and representation power of transformer architectures, DiTs have enabled impressive achievements across various applications, including image synthesis (Chen et al., 2023b), video generation (OpenAI, 2024), and multimodal content creation (Deng et al., 2025). However, the superior performance of DiTs comes at the cost of massive model size and computational complexity. As these models continue to scale, merely inference becomes prohibitively expensive, limiting their deployment in real-world scenarios. To generate a 512×512 video with only 16 frames, the OpenSORA (OpenAI, 2024) model, as an example, takes more than 50 seconds on an NVIDIA A100 GPU and consumes over 10GB.

Model Quantization (Jacob et al., 2018), as an indispensable step in deployment, can effectively compress model storage and accelerate inference. Converting high-bit-width floating-point (FP) numbers into low-bit-width integers (INT), model quantization can compress models by several times. Moreover, considering hardware architecture, the integer operations are usually simpler and more efficient than floating-point operations (Zhang et al., 2021), thereby allowing quantization to save bandwidth and accelerating computation (Liu et al., 2025). However, conversion from high-bit-width to low-bit-width also inevitably brings performance degradation due to the quantization error. Specifically, when considering DiTs in visual generation, quantization research is still underexplored (Wu et al., 2025). Previous research mainly focuses on high-bit quantization and suffers from extreme performance degradation when compressing to a lower bit-width (Zhao et al., 2025).

Specifically, when compressing to a lower bit-width, these methods usually suffer from the outliers in the network (Xiao et al., 2023). When considering the distribution, both weight and activation obey the bell distribution. Previous research demonstrates that the outliers’ impact on the performance is negligible (Liu et al., 2024a). However, it is not the case for DiTs. We observe that there are more extreme values in DiTs compared to low-level Transformer models. These extreme values exert a substantial influence during model quantization. First, they introduce significant rounding errors. A common approach to determine quantization boundaries is through the use of min–max or percentile methods (Liu et al., 2024b). Under both schemes, the resulting quantization ranges tend to be excessively large in absolute value, which amplifies rounding errors and thereby degrades model performance. Second, if one chooses to clip these extreme values, model performance can also be severely affected. This is because such extreme values often encode critical information that is essential to the generative process. Therefore, how to properly handle extreme values remains an open problem, as it has a profound impact on model performance.

In this work, we propose **CLQ** to compress visual generation models to ultra-low bit-width while preserving the high-quality output of the original model, as shown in Fig. 1. First, we begin with the analysis of the calibration process. Previous methods use the full-precision input and output of each module during calibration. However, quantization error accumulates as a discrepancy exists between the full-precision input data and the quantized ones. Therefore, we propose a novel cross-block calibration (CBC) method to obtain more accurate calibration data, thereby providing precise guidance in the following quantization process. Second, we propose orthogonal-based smoothing (OBS). OBS first detects the uneven channel and sorts the channels with an outlier score. Then, OBS smooths uneven activations and weight matrices using a block Hadamard transform, preventing outliers in irregular channels from affecting the more stable ones. In the quantization phase, we novelly propose cross-layer parameter searching (CLPS), which analyzes the most influenced layers and leverages cross-layer to obtain the quantization parameters with the minimum quantization error.

Combining both CBC, OBS, and CLPS, our proposed CLQ allows the model to still enjoy almost lossless performance. Moreover, when compressed into 4 bits, the model has a speedup of $3.95\times$, making it more applicable in real-world applications and deployment.

We summarize our contributions as follows:

- We propose cross-block calibration (CBC), a novel method for calibration data collection. CBC could provide accurate calibration data and minimize the accumulated quantization error, improving the quantized model’s performance.
- We propose orthogonal-based smoothing (OBS), which leverages rotation matrices to smooth the outliers and Hadamard matrices to be calculation-efficient.
- We propose cross-layer parameter searching (CLPS), which searches the quantization parameters with the second-order norm of the cross-layer output.
- We conduct extensive experiments to evaluate the proposed **CLQ** in visual generation tasks. We achieve W4A4 compression in visual generation and a $3.95\times$ speedup ratio with almost lossless model performance, pushing visual generation closer to real applications.

2 RELATED WORK

2.1 VISUAL GENERATION

Visual generation has progressed from early GAN-based (Goodfellow et al., 2020) methods to more stable diffusion models (Rombach et al., 2022). GANs, such as DCGAN (Radford et al., 2015) and StyleGAN (Karras et al., 2019), achieved impressive image realism but suffered from mode collapse and training instability. Variational autoencoders (Kingma & Welling, 2013) provided stable optimization but lower fidelity. Diffusion models changed the landscape, starting with DDPM (Ho et al., 2020) and later improvements like DDIM (Song et al., 2020) and classifier-free guidance (Ho & Salimans, 2022). These methods achieved state-of-the-art performance in image and video generation, showing robustness and controllability that surpassed previous paradigms.

2.2 DIFFUSION TRANSFORMER

The backbone of diffusion models was initially a U-Net architecture (Ronneberger et al., 2015). Recent works (Rombach et al., 2022) replaced U-Nets with Transformers (Vaswani et al., 2017) to improve scalability and representation. DiT showed that pure transformers could outperform convolutional backbones in diffusion tasks. PixArt- α Chen et al. (2023a) explores the fast training diffusion model with transformers, achieving photorealistic text-to-image synthesis. OpenSora OpenAI (2024), on the other hand, offers an efficient practice to generate videos with DiTs. These architectures enabled stronger scaling laws, similar to large language models, and unlocked new applications in high-resolution image synthesis and multi-modal generation. However, the increasing model size and complexity hinder the deployment in real-world, resource-constrained scenarios.

2.3 POST-TRAINING QUANTIZATION

Quantization (Jacob et al., 2018) has become a practical approach for compressing deep networks without retraining. Early PTQ methods, such as percentile quantization (Li et al., 2019), achieved efficiency but limited accuracy. Advanced PTQ methods like GPTQ (Frantar et al., 2022) and DuQuant (Lin et al., 2024) improved precision for large language models by handling activation outliers and optimizing quantization error. SmoothQuant Xiao et al. (2023) leverages diagonal matrices to smooth activation and transfer the quantization difficulties from activations to weights. ViDiT-Q Zhao et al. (2025) presents a successful practice for PTQ on visual generation tasks. However, these current PTQ methods collapse when it comes to ultra-low bit-width, such as W4A4. One way to compensate for the quantization loss is to use finer quantization granularity, which also slows the inference. Therefore, applying PTQ to DiT models remains an open question. This motivates research on PTQ tailored for DiTs, especially for visual generation tasks.

3 METHOD

3.1 PRELIMINARY

Post-training quantization (PTQ) reduces model precision without retraining. A common practice is asymmetric uniform quantization, which achieves a trade-off between hardware ecosystem and

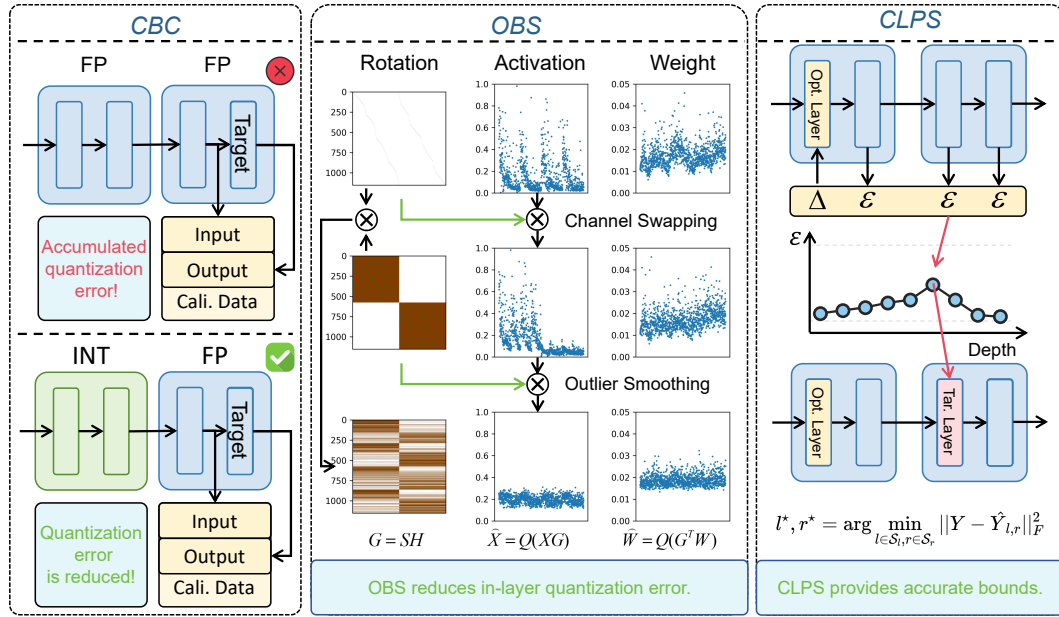


Figure 2: The overall pipeline of the proposed CLQ, which consists of three novel designs. CBC provides accurate calibration data and reduces the accumulated quantization error. OBS leverages column-swapping matrices and block Hadamard matrices to smooth the outliers with negligible overhead in inference and storage. CLPS analyzes the sensitive target layer and reduces the cross-layer quantization error. All three methods together guarantee the outstanding performance.

model performance. Given a full-precision weight $\mathbf{W} \in \mathbb{R}$, it is mapped into a quantized value $\hat{\mathbf{W}}$ by

$$\hat{\mathbf{W}} = Q(\mathbf{W}, l, r, n) = \text{Round} \left(\frac{\text{Clip}(\mathbf{W}, l, r) - l}{r - l} \cdot (2^n - 1) \right) \cdot \frac{r - l}{2^n - 1}, \quad (1)$$

where l and r are left and right bounds for quantization, n is the number of bits, $\text{Clip}(\cdot)$ clamps the input value into the given range, and $\text{Round}(\cdot)$ rounds the values into the nearest integers. Eq. 1 allows for stimulating the quantization error without the deployment. Both weights and activations can be quantized in this manner. Previous works set $l = \min(\mathbf{W})$, $r = \max(\mathbf{W})$ directly, which is not appropriate for DiTs. In our work, l and r are the quantization parameters to be optimized. n is assigned as a fixed given value. To be brief, W4A8 is short for quantizing the weights into 4 bits and activations into 8 bits. We adopt the dynamic quantization, where the l and r for activations are calculated dynamically according to the input, and the weights are only quantized once.

3.2 CROSS-BLOCK CALIBRATION

In the PTQ process, a critical step is collecting data to analyze the distribution of model activations, which subsequently guides the optimization of the model's quantization parameters. This procedure is referred to as calibration, and the data used is known as the calibration set. Previous approaches typically involve collecting full-precision activations across the entire network at once and calibrating the quantization parameters using full-precision inputs and outputs. However, this method leads to the layer-by-layer accumulation of quantization errors, which impacts the model's performance.

Previous methods aim to find the quantization parameters φ with activation \mathbf{X} , weights \mathbf{W} , and the output $\mathbf{Y} = \mathbf{XW}$. However, quantization compresses the weight of all the layers, leading to a mismatch between the quantized weights and the original ones. Therefore, the outputs of layers change significantly. Moreover, considering that the input of the target layer is the output of the previous layer, the input has changed to $\hat{\mathbf{X}}$ when calibrating the target layer. Further, the changes of the input accumulate as the calibration goes deeper, leading to a significant calibration error.

To address this problem, we propose cross-block calibration (CBC) to obtain accurate calibration data, with which the quantization can be better guided. First, when collecting the calibration data, all previous layers must be properly quantized. Here, “properly” refers to adopting the proposed PTQ method. Only then can we reduce the quantization error to the best extent. Considering the

limited depth of one transformer block, we choose a coarser granularity for easier implementation. To be specific, when collecting the target layer’s calibration data, we only require that the previous transformer blocks is quantized instead of all the layers ahead.

3.3 ORTHOGONAL-BASED SMOOTHING

Smoothing the model through rotation matrices has been proven to be an efficient method (Liu et al., 2024b). However, previous studies (Lin et al., 2024; Ashkboos et al., 2024) typically adopted dynamic approaches to construct the rotation matrix, which are time-consuming and hardware-unfriendly. In contrast, we novelly propose using a static approach to further enhance the role of rotation matrices.

Data Preparing. Specifically, we have obtained the activation data $X \in \mathbb{R}^{B \times N \times D}$ of the target layer from CBC, where B is the batch size, N is the number of tokens, and D is the number of channels. First, we observe that the activations form stable statistical characteristics along the batch dimension. We then average X along the batch dimension, resulting in the statistical mean matrix $S \in \mathbb{R}^{N \times D}$, where N is fixed during the process of image or video generation.

Outlier Detection. Following the approach of DuQuant (Lin et al., 2024), we utilize an outlier metric to assess the outliers across different channels. Specifically, we define the outlier metric for each channel as the absolute maximum value of the activations in that channel. We then sort the outlier metrics in descending order and construct a column-swapping matrix: the top 50% of channels are moved to the left side, and the bottom 50% to the right side. Thus, the left side consists of high-peak channels, while the right side consists of low-peak channels. We also experimented with other metrics, such as variance and range, but the final experimental results showed no significant differences (See ablation part). Therefore, we adopted the simplest form, *i.e.*, the absolute maximum value.

Orthogonal Smoothing. Next, we construct an orthogonal rotation matrix, which is a block Hadamard matrix \mathbf{H} , and multiply it by the column-swapping matrix \mathbf{S} to obtain the total orthogonal transformation matrix $\mathbf{G} = \mathbf{SH}$. The column-swapping matrix gathers the outliers together, and the Hadamard matrix could effectively smooth the activation matrix by rotating the outliers into smooth parts. Together, \mathbf{G} reduces quantization error and improves model performance effectively.

Overhead Analysis. \mathbf{G} is stored as part of the quantization parameters and is invoked during inference. As \mathbf{G} is an orthogonal matrix, *i.e.*, $\mathbf{GG}^T = \mathbf{I}$, it brings lossless smoothing. For weights, \mathbf{G} can be directly absorbed into the weights before quantization by $\hat{\mathbf{W}} = Q(\tilde{\mathbf{W}}) = Q(\mathbf{G}^T \mathbf{W})$, which does not incur additional storage overhead. For activations, since the matrix is a block Hadamard matrix, the matrix multiplication can be performed using fast Hadamard multiplication with a time complexity of $\mathcal{O}(n^2 \log n)$, where n is typically in the thousands. Hence, compared to the subsequent matrix multiplication with a time complexity of $\mathcal{O}(n^3)$, this step can be ignored.

As for storage, Hadamard matrices enjoy excellent properties. (1) It can be generated online, saving disk storage. (2) The Hadamard matrices’ elements are binary, *i.e.*, ± 1 , saving GPU memory. We only need to store the column-swapping matrix \mathbf{S} , which can be further compressed into a vector \mathbf{s} , with its k -th element indexing the column after swapping. Considering D is huge for most of the layers, the storage overhead of \mathbf{s} is usually less than 0.1%, which can be safely ignored.

Additionally, in the outlier channel swapping, we do not need an overall descending order because this approach facilitates the multiplication with the block Hadamard matrix. The rotation matrix takes the form of a block diagonal matrix, where each block processes 50% of the columns of the activation. Therefore, we only need to swap the columns with higher outlier values to the same side, without forcing the arrangement into descending order. Moreover, the blocked form also fastens the calculation. More detailed analysis can be found in the supplementary material.

3.4 CROSS-LAYER PARAMETER SEARCHING

In most existing studies, the quantizer parameters, namely l and r , have received little attention, despite their significant impact on quantization outcomes. Recent approaches (Zhao et al., 2025) typically adopt simple strategies such as min–max or percentile bounds. However, such coarse methods often result in severe degradation or even collapse under low-bit quantization. To address this issue, we propose **CLPS**, a cross-layer parameter searching method.

The essence of optimizing quantizer parameters lies in minimizing the adverse effects of rounding and clipping errors on model performance. Directly relying on the final model output for this optimization would be computationally prohibitive, as each layer would require a complete forward pass, and the

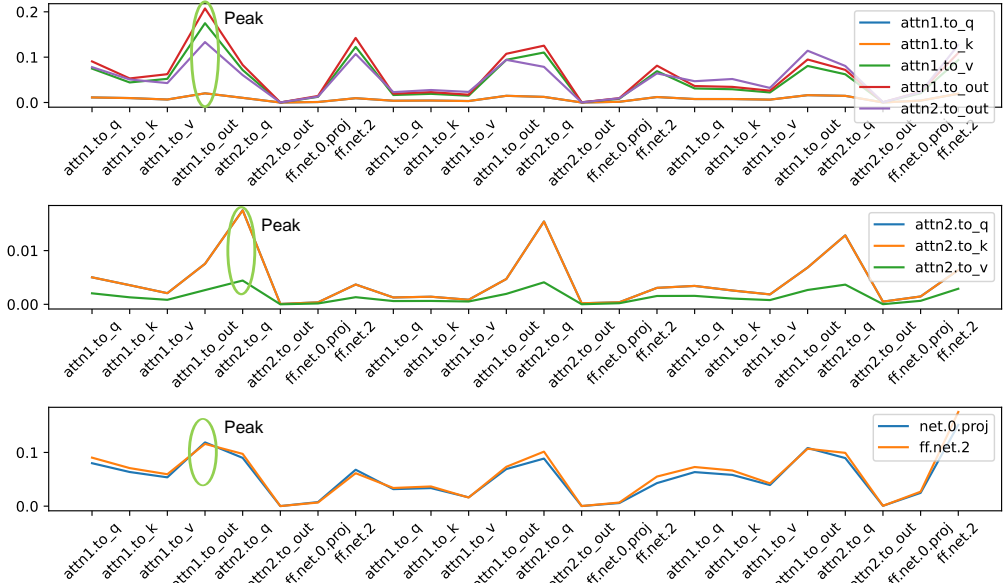


Figure 3: The visualization of cross-layer error when giving a disturbance to stimulate quantization error. For each layer to be optimized, we analyze the most influenced layer, *i.e.*, the peak, with the shift from the original output, and set it as the target layer for quantization parameter optimization.

VAE part needs to be included, which is computationally expensive. On the other hand, using only the local input and output of a given layer would be insufficient to capture its potential influence.

To balance these considerations, our principle is to select, around the layer to be optimized, the subsequent layer exhibiting the largest variance as the target layer. We limit the target layer to be within the subsequent three blocks. To find the target layer, we apply perturbations to the layer to be optimized and perform forward propagation to obtain the output of all the subsequent layers. Perturbations lead to a shift from the original output. We quantify the shift as the L1 norm between the shifted output \tilde{y}_{L_t} and the original output y_{L_t} of the subsequent layer L_t . We determine the target layer as the most influenced layer, which can be written as

$$L_T = \arg \max_{L_t} \|\tilde{y}_{L_t} - y_{L_t}\|_1. \quad (2)$$

Once the optimized layer L_O and the target layer L_T are determined, we perform a grid search over the $l \in \mathcal{S}_l = [Q_\beta(W_{L_O}), Q_\gamma(W_{L_O})]$ and $r \in \mathcal{S}_r = [Q_{1-\gamma}(W_{L_O}), Q_{1-\beta}(W_{L_O})]$, where $Q_\eta(W)$ is the $\eta\%$ greatest value of W , β and γ are the grid bounds. The search objective is defined as

$$l^*, r^* = \arg \min_{l \in \mathcal{S}_l, r \in \mathcal{S}_r} \|Y - \hat{Y}_{l,r}\|_F^2, \quad (3)$$

where Y is the original output of L_T and $\hat{Y}_{l,r}$ is the output of L_T after quantizing L_O with l and r . With CLPS, the cross-layer quantization error on the most influenced layer can be minimized.

3.5 OVERALL

We propose three designs, which are CBC for accurate calibration, OBS for outlier smoothing, and CLPS for determining quantization parameters. Here, we introduce the sequence of these three designs. Overall, we perform CBC, OBS, and CLPS iteratively across Transformer blocks. When quantizing the k -th Transformer block B_k , the previous blocks are already properly quantized. We first perform CBC to collect the calibration data. Then, we quantize the layer inside the Transformer block one by one. Given a layer to be optimized L_O , we first determine the rotation matrix \mathbf{G} in OBS and merge it into the weight matrix. Then, we find the corresponding target layer L_T and perform CLPS to obtain l^* and r^* for L_O . For the last Transformer block, the target layer is set to be the output of the block. The pseudocode is provided in the supplementary materials.

4 EXPERIMENTS

4.1 EXPERIMENTAL SETTINGS

Video Generation Evaluation Settings. We apply **CLQ** to Open-Sora 1.2 to test the video generation task. All the videos are generated with 100 steps with a CFG scale of 4.0. The evaluation of **CLQ** is

Table 1: Ablation study on our proposed designs, including CBC, OBS, and CLPS. The results on all metrics demonstrate the effectiveness of the proposed designs.

Method	Single Object	Two Object	Counting	Colors	Position	Color Attribute	Total
Naive	0.934	0.525	0.425	0.722	0.050	0.050	0.451
+OBS	0.978	0.525	0.425	0.917	0.200	0.250	0.549
+CLPS	0.978	0.575	0.425	0.917	0.275	0.250	0.570
+CBC	0.978	0.625	0.425	0.944	0.300	0.275	0.591

Table 2: Ablation of five outlier metrics on GenEval. No obvious difference is observed.

Method	Single Object	Two Object	Counting	Colors	Position	Color Attribute	Total
Abs Max	0.972	0.650	0.425	0.917	0.225	0.375	0.594
Percentile	0.978	0.600	0.450	0.944	0.275	0.250	0.583
Top k Mean	0.972	0.650	0.425	0.917	0.225	0.375	0.594
Range	0.978	0.625	0.425	0.917	0.250	0.325	0.587
PAR	0.975	0.575	0.425	0.917	0.275	0.325	0.582

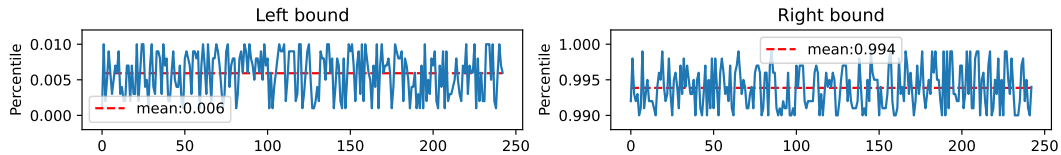


Figure 4: The left and right bound, *i.e.*, quantization parameters of CLPS on PixArt- α .

performed on VBenH Huang et al. (2024) to provide comprehensive results. Following previous research Zhao et al. (2025), we select 7 major dimensions from VBenH, including imaging quality, aesthetic quality, motion smoothness, dynamic degree, background consistency, scene consistency, and overall consistency. The result of the other dimensions are in the supplementary material.

Image Generation Evaluation Settings. We apply **CLQ** to PixArt- α Chen et al. (2023a) to test the image generation task. When evaluating, the images are generated with a 50-step DPM-solver with the CFG scale of 4.5. We adopt GenEval Ghosh et al. (2023) to evaluate the performance, and all its metrics are reported, including single object, two object, counting, colors, position, attribute binding, and overall. With all these metrics, the performance of our **CLQ** can be thoroughly evaluated.

Quantization Scheme. The quantization granularity is set to be per-channel. We test the performance of **CLQ** under three bit settings, including W8A8, W4A8, and W4A4. As the matrices are smoothed enough after OBS, we set the percentile the same for all channels within a matrix in CLPS. We set $\beta = 0, \gamma = 0.01$ for CLPS. To demonstrate the performance of **CLQ**, we select the SOTA PTQ methods for comparison, including ViDiT-Q (Zhao et al., 2025), SmoothQuant (Xiao et al., 2023), QuaRot (Ashkboos et al., 2024), and Q-DiT (Chen et al., 2025).

4.2 ABLATION STUDY

We present ablation studies in Tab. 1 to evaluate the contribution of the different components in the proposed **CLQ**. The ablation study is conducted on a subset of GenEval. By randomly choosing the prompts, the generated images are enough to cover different dimensions while requiring less computation. We provide the prompts used in the supplementary material.

Evaluation of OBS. As shown in Tab. 1, the proposed OBS could effectively smooth the activation matrix. The quantization error of both weights and activations is reduced 90% compared to those before OBS. Moreover, we also provide a visualization of the activations and weights before and after OBS in the supplementary material, which also supports the obvious smoothing ability of OBS. Therefore, OBS improves the performance of the quantized model with negligible overhead.

Evaluation of CLPS. Next, we evaluate the effectiveness of CLPS. After searching for the optimized quantization parameters, the model’s performance enjoys obvious improvement. Fig. 3 shows the distribution of the searched parameters along the model depth. The average bound across the whole model is (0.006, 0.994). Both compact results validate the necessity of optimizing the bound.

Evaluation of CBC. Next, we incorporate CBC alongside the other designs. The block-wise calibration data provide an accurate guide to OBS and CLPS, further enhancing model performance.

Table 3: Comparison with SOTA PTQ methods on GenEval. The best and the second best results are marked with **bold** and underline, respectively. “-” means the model collapses.

Method	Bits (W/A)	Single Object	Two Object	Counting	Colors	Position	Color Attribute	Total
FP	16/16	0.980	0.660	0.510	0.780	0.140	0.220	0.550
Q-DiT	8/8	0.981	0.612	0.525	0.750	0.113	0.150	0.522
SmoothQuant	8/8	0.969	<u>0.638</u>	0.450	<u>0.813</u>	<u>0.135</u>	0.163	0.528
Quarot	8/8	0.981	0.663	0.438	0.788	<u>0.135</u>	0.175	0.530
ViDiT-Q	8/8	0.978	0.634	0.463	0.793	<u>0.135</u>	0.210	0.535
CLQ (Ours)	8/8	0.975	0.663	0.463	0.815	0.150	0.210	0.546
Q-DiT	4/8	-	-	-	-	-	-	-
SmoothQuant	4/8	0.666	0.350	0.238	0.513	0.063	0.163	0.332
Quarot	4/8	0.772	<u>0.613</u>	0.363	0.588	0.088	0.175	0.433
ViDiT-Q	4/8	<u>0.891</u>	0.475	0.406	<u>0.649</u>	<u>0.108</u>	0.208	0.456
CLQ (Ours)	4/8	0.975	0.649	0.472	0.763	0.125	0.235	0.537
Q-DiT	4/4	-	-	-	-	-	-	-
SmoothQuant	4/4	-	-	-	-	-	-	-
Quarot	4/4	0.219	<u>0.063</u>	0.038	0.138	<u>0.038</u>	0.013	0.084
ViDiT-Q	4/4	<u>0.247</u>	0.035	<u>0.038</u>	<u>0.165</u>	0.008	<u>0.018</u>	<u>0.085</u>
CLQ (Ours)	4/4	0.938	0.614	0.456	0.736	0.108	0.200	0.509

Table 4: Comparison with SOTA PTQ methods on VBench. The best and the second best results are marked with **bold** and underline, respectively. “-” means the model collapses.

Methods	Bits (W/A)	Imaging Quality	Aesthetic Quality	Motion Smooth.	Dynamic Degree	BG. Consist.	Scene Consist.	Overall Consist.
FP	16/16	56.45	55.48	98.49	51.39	97.36	45.20	26.91
Q-DiT	8/8	54.28	<u>55.80</u>	93.64	40.27	94.70	33.35	26.09
SmoothQuant	8/8	<u>55.38</u>	55.38	98.12	37.50	97.01	36.01	26.49
Quarot	8/8	55.37	55.38	98.20	37.50	97.26	32.31	26.59
ViDiT-Q	8/8	55.92	54.66	98.43	50.00	<u>97.10</u>	41.56	26.66
CLQ (Ours)	8/8	55.37	55.89	<u>98.28</u>	<u>41.67</u>	97.61	<u>36.41</u>	<u>26.62</u>
Q-DiT	4/8	23.30	29.61	97.89	4.16	97.02	0.00	4.98
SmoothQuant	4/8	51.47	54.87	98.11	34.72	96.76	31.35	26.22
Quarot	4/8	50.97	<u>54.96</u>	<u>98.18</u>	33.33	96.73	<u>31.92</u>	<u>26.70</u>
ViDiT-Q	4/8	53.16	53.04	98.28	44.44	<u>97.30</u>	31.82	26.29
CLQ (Ours)	4/8	54.79	55.81	<u>98.18</u>	<u>41.67</u>	97.75	32.85	26.71
Q-DiT	4/4	-	-	-	-	-	-	-
SmoothQuant	4/4	<u>40.41</u>	<u>37.82</u>	84.63	100.00	93.81	0.00	3.57
Quarot	4/4	<u>38.22</u>	<u>36.45</u>	92.12	100.00	94.16	0.02	<u>5.01</u>
ViDiT-Q	4/4	38.52	37.72	<u>92.71</u>	100.00	<u>94.70</u>	<u>0.44</u>	4.67
CLQ (Ours)	4/4	50.69	54.14	97.42	36.11	95.94	31.69	26.33

Choice of Outlier Metric. In OBS, we need to determine the outlier score of each channel. We test five commonly used metrics, including absolute max value, percentile, top k mean, range, and peak average ratio (PAR). We set the percentile as (1%, 99%) and $k = 1\%$ in top k mean. As shown in Tab. 2, there is no evident difference between the tested metrics. Therefore, we select the simplest form, *i.e.*, absolute maximum value, which also enjoys excellent performance on most metrics.

Target Layer of CLPS. We observe that the target layer of CLPS is stable when considering the model structure. Take OpenSora as an example, the target layer is always the attn1.to_out in the next block for layers in attn1, attn2.to_out, and layers in FFN, as shown in Fig. 3. And it is always the attn1.to_q in the next block for the rest of the layers in attn2. Therefore, fixing the target layer during quantization is an optional and feasible way to speed up the PTQ process.

4.3 COMPARISON WITH STATE-OF-THE-ART METHODS

Tab. 3 shows the results on image generation, and Tab. 4 shows the results on video generation. Our proposed CLQ consistently performs the best or the second best on all metrics when it comes to the low-bit scenario. The dynamic degree is an exception. When compressed to W4A4, the generated videos of the compared methods are full of random noise, which brings a high dynamic degree of 100. Therefore, there is a sweet spot for video quality when evaluated on VBench. These outstanding results demonstrate the effectiveness and robustness of the proposed CLQ.

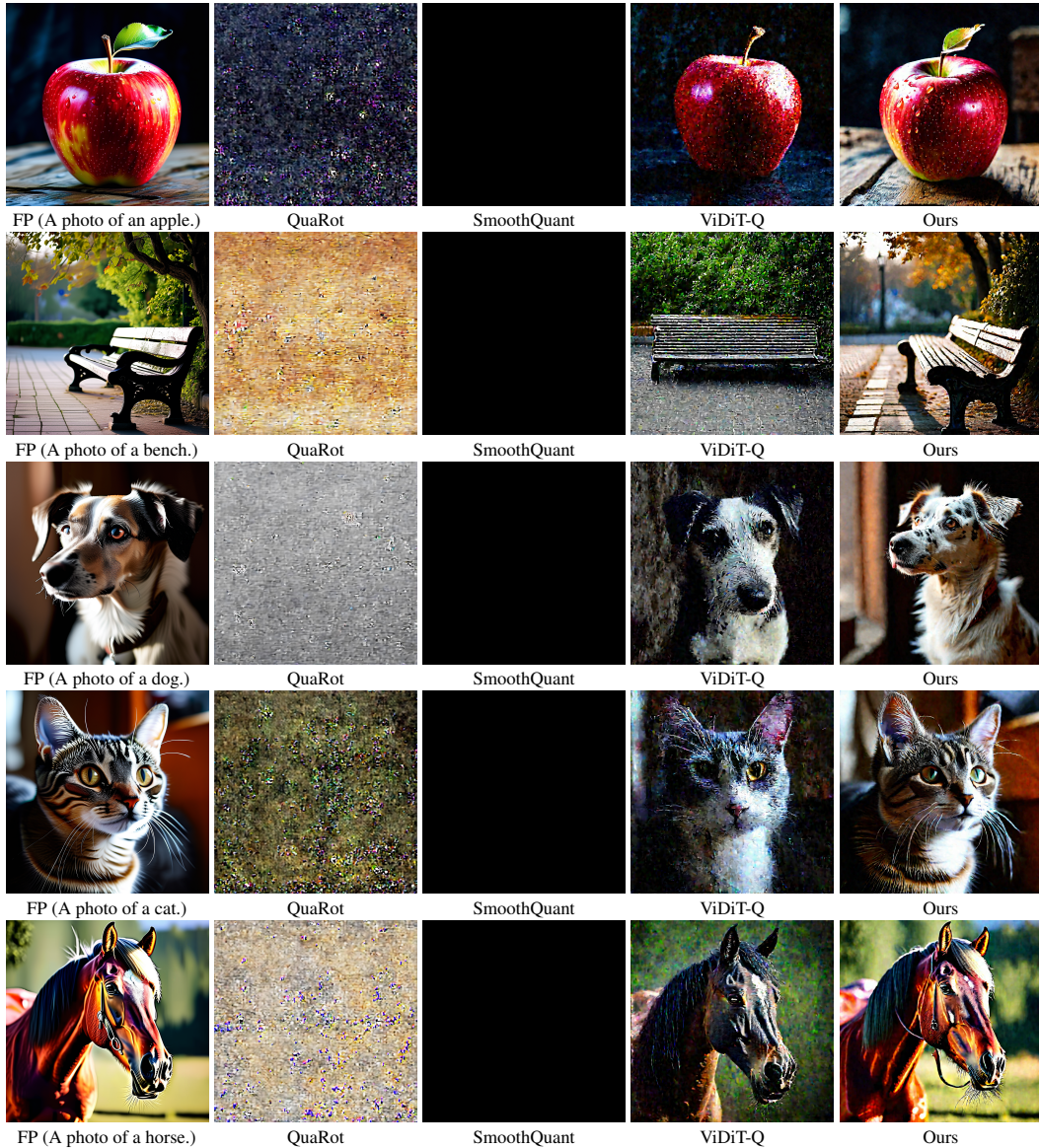


Figure 5: Visual comparison for generation with **W4A4**. We compare our proposed CLQ with current competitive PTQ methods and the full-precision (FP) model. The visual results illustrate that CLQ follows the prompt accurately and gains rich details and less noise.

Fig. 5 shows the generated visual contents of the proposed CLQ and the SOTA methods under ultra-low bit-width, *i.e.*, W4A4. SmoothQuant can only generate all black content, while QuaRot generates random noise. Both methods collapse due to the severe precision loss after quantization. ViDiT-Q can keep the semantic contents according to the text prompts, but obvious noise can be observed around the whole image. In contrast, our results are visually the same as the FP model, representing the excellent performance of the proposed CLQ. More results are in the supplementary materials. Both quantitative and qualitative results demonstrate the effectiveness of CLQ.

5 CONCLUSION

We propose CLQ, an efficient post-training method for visual generation models. CLQ consists of three novel designs, including CBC, OBS, and CLPS. CBC provides accurate calibration data for the other two components. OBS leverages the Hadamard matrix to smooth the outliers with negligible overhead. CLPS searches for the quantization parameters with the most influenced subsequent layer. All three designs together enable the visual generation model to provide FP-similar content when compressed to W4A4. Future work will focus on lower bit-width and further improving performance.

REFERENCES

Saleh Ashkboos, Amirkeivan Mohtashami, Maximilian L Croci, Bo Li, Pashmina Cameron, Martin Jaggi, Dan Alistarh, Torsten Hoefer, and James Hensman. Quarot: Outlier-free 4-bit inference in rotated llms. *NeurIPS*, 2024.

Junsong Chen, Jincheng Yu, Chongjian Ge, Lewei Yao, Enze Xie, Yue Wu, Zhongdao Wang, James Kwok, Ping Luo, Huchuan Lu, et al. Pixart- α : Fast training of diffusion transformer for photorealistic text-to-image synthesis. *arXiv preprint arXiv:2310.00426*, 2023a.

Junsong Chen, Jincheng Yu, Chongjian Ge, Lewei Yao, Enze Xie, Yue Wu, Zhongdao Wang, James Kwok, Ping Luo, Huchuan Lu, et al. Pixart- α : Fast training of diffusion transformer for photorealistic text-to-image synthesis. *arXiv preprint arXiv:2310.00426*, 2023b.

Lei Chen, Yuan Meng, Chen Tang, Xinzhu Ma, Jingyan Jiang, Xin Wang, Zhi Wang, and Wenwu Zhu. Q-dit: Accurate post-training quantization for diffusion transformers. In *CVPR*, 2025.

Chaorui Deng, Deyao Zhu, Kunchang Li, Chenhui Gou, Feng Li, Zeyu Wang, Shu Zhong, Weihao Yu, Xiaonan Nie, Ziang Song, et al. Emerging properties in unified multimodal pretraining. *arXiv preprint arXiv:2505.14683*, 2025.

Elias Frantar, Saleh Ashkboos, Torsten Hoefer, and Dan Alistarh. Gptq: Accurate post-training quantization for generative pre-trained transformers. *arXiv preprint arXiv:2210.17323*, 2022.

Dhruba Ghosh, Hannaneh Hajishirzi, and Ludwig Schmidt. Geneval: An object-focused framework for evaluating text-to-image alignment. *NeurIPS*, 2023.

Ian Goodfellow, Jean Pouget-Abadie, Mehdi Mirza, Bing Xu, David Warde-Farley, Sherjil Ozair, Aaron Courville, and Yoshua Bengio. Generative adversarial networks. *Communications of the ACM*, 2020.

Jonathan Ho and Tim Salimans. Classifier-free diffusion guidance. *arXiv preprint arXiv:2207.12598*, 2022.

Jonathan Ho, Ajay Jain, and Pieter Abbeel. Denoising diffusion probabilistic models. *NeurIPS*, 2020.

Ziqi Huang, Yinan He, Jiashuo Yu, Fan Zhang, Chenyang Si, Yuming Jiang, Yuanhan Zhang, Tianxing Wu, Qingyang Jin, Nattapol Chanpaisit, et al. Vbench: Comprehensive benchmark suite for video generative models. In *CVPR*, 2024.

Benoit Jacob, Skirmantas Kligys, Bo Chen, Menglong Zhu, Matthew Tang, Andrew Howard, Hartwig Adam, and Dmitry Kalenichenko. Quantization and training of neural networks for efficient integer-arithmetic-only inference. In *CVPR*, 2018.

Tero Karras, Samuli Laine, and Timo Aila. A style-based generator architecture for generative adversarial networks. In *CVPR*, 2019.

Diederik P Kingma and Max Welling. Auto-encoding variational bayes. *arXiv preprint arXiv:1312.6114*, 2013.

Rundong Li, Yan Wang, Feng Liang, Hongwei Qin, Junjie Yan, and Rui Fan. Fully quantized network for object detection. In *CVPR*, 2019.

Haokun Lin, Haobo Xu, Yichen Wu, Jingzhi Cui, Yingtao Zhang, Linzhan Mou, Linqi Song, Zhenan Sun, and Ying Wei. Duquant: Distributing outliers via dual transformation makes stronger quantized llms. *NeurIPS*, 2024.

Kai Liu, Haotong Qin, Yong Guo, Xin Yuan, Linghe Kong, Guihai Chen, and Yulun Zhang. 2dquant: Low-bit post-training quantization for image super-resolution. *NeurIPS*, 2024a.

Kai Liu, Qian Zheng, Kaiwen Tao, Zhiteng Li, Haotong Qin, Wenbo Li, Yong Guo, Xianglong Liu, Linghe Kong, Guihai Chen, et al. Low-bit model quantization for deep neural networks: A survey. *arXiv preprint arXiv:2505.05530*, 2025.

Zechun Liu, Changsheng Zhao, Igor Fedorov, Bilge Soran, Dhruv Choudhary, Raghuraman Krishnamoorthi, Vikas Chandra, Yuandong Tian, and Tijmen Blankevoort. Spinquant: Llm quantization with learned rotations. *arXiv preprint arXiv:2405.16406*, 2024b.

OpenAI. Video generation models as world simulators. <https://openai.com/index/video-generation-models-as-world-simulators/>, 2024.

William Peebles and Saining Xie. Scalable diffusion models with transformers, 2023.

Alec Radford, Luke Metz, and Soumith Chintala. Unsupervised representation learning with deep convolutional generative adversarial networks. *arXiv preprint arXiv:1511.06434*, 2015.

Robin Rombach, Andreas Blattmann, Dominik Lorenz, Patrick Esser, and Björn Ommer. High-resolution image synthesis with latent diffusion models. In *CVPR*, 2022.

Olaf Ronneberger, Philipp Fischer, and Thomas Brox. U-net: Convolutional networks for biomedical image segmentation. In *MICCAI*. Springer, 2015.

Uriel Singer, Adam Polyak, Thomas Hayes, Xiaoyue Yin, Jie An, Songyang Zhang, Qiyuan Hu, Harry Yang, Oron Ashual, Oran Gafni, Devi Parikh, Sonal Gupta, and Yaniv Taigman. Make-a-video: Text-to-video generation without text-video data. *arXiv*, abs/2209.14792, 2022.

Jiaming Song, Chenlin Meng, and Stefano Ermon. Denoising diffusion implicit models. *arXiv preprint arXiv:2010.02502*, 2020.

Ashish Vaswani, Noam Shazeer, Niki Parmar, Jakob Uszkoreit, Llion Jones, Aidan N Gomez, Łukasz Kaiser, and Illia Polosukhin. Attention is all you need. *NeurIPS*, 30, 2017.

Junyi Wu, Zhiteng Li, Zheng Hui, Yulun Zhang, Linghe Kong, and Xiaokang Yang. Quantcache: Adaptive importance-guided quantization with hierarchical latent and layer caching for video generation. *arXiv preprint arXiv:2503.06545*, 2025.

Guangxuan Xiao, Ji Lin, Mickael Seznec, Hao Wu, Julien Demouth, and Song Han. Smoothquant: Accurate and efficient post-training quantization for large language models. In *ICML*. PMLR, 2023.

Jintao Zhang, Gang Li, Yongshun Luo, and Ling Lin. Higher precision integer operations instead of floating-point operations in computers or microprocessors. *Review of Scientific Instruments*, 2021.

Tianchen Zhao, Tongcheng Fang, Haofeng Huang, Enshu Liu, Rui Wan, Widayadewi Soedarmadji, Shiyao Li, Zinan Lin, Guohao Dai, Shengen Yan, et al. Vudit-q: Efficient and accurate quantization of diffusion transformers for image and video generation. In *ICLR*, 2025.